Cross Calibration of SDGSAT-1/TIS Thermal Infrared Bands With FY-4A/AGRI

Min Zhu, Xue Zhao, Lu Zou, Fansheng Chen, and Zhuoyue Hu

***Abstract*—Launched in November 2021, the sustainable development science satellite-1 carries the thermal infrared spectrometer (TIS) as a pivotal payload. Achieving precise radiometric calibration for geophysical parameter accuracy is crucial. Leveraging the frequent cross-calibration capability of the geostationary satellite FY-4A/advanced geostationary radiation imager (AGRI), this study addresses observational geometry challenges. The proposed radiance correction model for FY-4A/AGRI effectively reduces radiance discrepancies caused by differences in satellite zenith angles between TIS and AGRI. After integrating the corrected data into nadir-observed statistics, the long-term brightness temperature (BT) bias of TIS and AGRI was monitored. The results show that the daytime and nighttime BT bias exhibit similar trends, with the *B*2 band mainly showing negative bias. Overall, the BT bias for the *B*2 and *B*3 bands is within 1 K. The standard deviation of the BT bias for approximately 2250 sample points was calculated, revealing the values of 0.22 K and 0.40 K during the daytime, and 0.31 K and 0.57 K at night. The introduced model error remains below 0.31 K. Regarding the uncertainty of the BT bias introduced by spectral matching, when the spectral broadening is 1.15 times the wavelength interval, the uncertainty is less than 0.29 K for *B*2 and less than 0.38 K for *B*3. This work enhances our understanding of radiometric calibration challenges, providing insights into satellite-based geophysical parameter accuracy.**

***Index Terms*—Advanced geostationary radiation imager (AGRI), cross calibration, sustainable development science satellite-1/thermal infrared spectrometer (SDGSAT-1/TIS), thermal infrared (TIR), zenith angle correction.**

Manuscript received 29 December 2023; revised 29 February 2024 and 12 April 2024; accepted 29 April 2024. Date of publication 2 May 2024; date of current version 23 May 2024. This work was supported in part by the Strategic Priority Research Program of the Chinese Academy of Sciences under Grant XDA19010102 and in part by the National Natural Science Foundation of China under Grant 61975222. *(Corresponding author: Fansheng Chen.)*

Min Zhu and Xue Zhao are with the Key Laboratory of Intelligent Infrared Perception, Shanghai Institute of Technical Physics, Chinese Academy of Sciences, Shanghai 200083, China, and also with the University of Chinese Academy of Sciences, Beijing 100049, China (e-mail: zhumin@mail.sitp.ac.cn; zhaoxue22@mails.ucas.ac.cn).

Lu Zou is with the State Key Laboratory of Astronautic Dynamics, China Xi'an Satellite Control Center, Xi'an 710043, China (e-mail: 13351813101@189.cn).

Fansheng Chen is with the Key Laboratory of Intelligent Infrared Perception, Shanghai Institute of Technical Physics, Chinese Academy of Sciences, Shanghai 200083, China, also with the International Research Center of Big Data for Sustainable Development Goals (CBAS), Beijing 100094, China, and also with the Hangzhou Institute for Advanced Study, University of Chinese Academy of Sciences, Hangzhou 310024, China (e-mail: cfs@mail.sitp.ac.cn).

Zhuoyue Hu is with the Key Laboratory of Intelligent Infrared Perception, Shanghai Institute of Technical Physics, Chinese Academy of Sciences, Shanghai 200083, China (e-mail: huzhuoyue@mail.sitp.ac.cn).

Digital Object Identifier 10.1109/JSTARS.2024.3396228

I. Introduction

THE Sustainable Development Science Satellite-1 (SDGSAT-1) is the world's first scientific satellite dedicated to serving the 2030 agenda for sustainable development. Equipped with three optical imagers, namely the thermal infrared spectrometer (TIS), multispectral imager for inshore, and glimmer imager for urbanization, it enables long-term continuous observation of the Earth. The TIS, with a resolution of 30 m and a swath width of 300 km, is a critical payload aboard SDGSAT-1 [1]. TIS features three long-wave infrared bands: *B*1 (8.0–10.5 μm), *B*2 (10.3–11.3 μm), and *B*3 (11.5–12.5 μm), as shown in Table I. In comparison with other thermal infrared (TIR) sensors, TIS stands out due to its higher resolution and wider swath width. The data generated by TIS are valuable for applications in environmental monitoring and ecological assessment, establishing its significance in advancing our understanding of Earth's dynamics in support of sustainable development goals.

According to the prelaunch testing results, TIS exhibited excellent performance, with noise equivalent temperature difference (NEdT) values of 0.034 K, 0.047 K, and 0.076 K for the three bands at 300 K, respectively.[1]. Ensuring the reliability and sustainable development of research and applications in the field of radiometry hinges on precise radiometric calibration. Calibration coefficients can be obtained through prelaunch laboratory experiments. However, after launch, satellite sensors may degrade over time due to changes in the satellite's environment, leading to potential alterations in sensor calibration coefficients. Cross calibration provides an effective method for selecting appropriate reference instruments, facilitating quality assessment, stability monitoring, uncertainty analysis, and calibration corrections for the target instrument [2].

Meteorological satellites equipped with remote sensing instruments enable long-term continuous Earth observation. FY-4A is China's second-generation geostationary orbit meteorological satellite. The advanced geostationary radiation imager (AGRI) is a primary instrument on the FY-4A satellite. Featuring a precisely designed dual-mirror structure, AGRI conducts accurate and flexible sensing in rapid sector scans at 2-D and small-scale levels. It comprises 14 spectral bands, with a 1-km resolution in the visible-near-infrared band, 2-km resolution in the shortwave infrared bands, and a 4-km resolution in the TIR bands [3]. In terms of spatial and temporal resolution, AGRI surpasses its predecessor, the S-VISSR radiometer on the FY2 series satellites, which had one visible light and four

TABLE I
INSTRUMENT CHARACTERISTICS OF SDGSAT-1/TIS AND FY-4A/AGRI

	SDGSAT-1/TIS	FY-4A/AGRI
Orbit Type	Sun-synchronous Orbit	Geostationary Orbit
Orbital Altitude	505 km	35 800 km
Orbital Inclination	97.5°	0°
Spatial Resolution	30 m	4 km
TIR Band	B1: 8.0–10.5 μm B2: 10.3–10.3 μm B3: 11.5–12.5 μm	CH_11: 8.0–9.0 μm CH_12: 10.3–11.3 μm CH_13: 11.5–12.5 μm CH_14: 13.2–13.8 μm
Sensitivity NEdT@300 K	B1: 0.034 K B2: 0.047 K B3: 0.076 K	CH_11: ⩽0.2 K CH_12: ⩽0.2 K CH_13: ⩽0.2 K CH_14: ⩽0.5 K

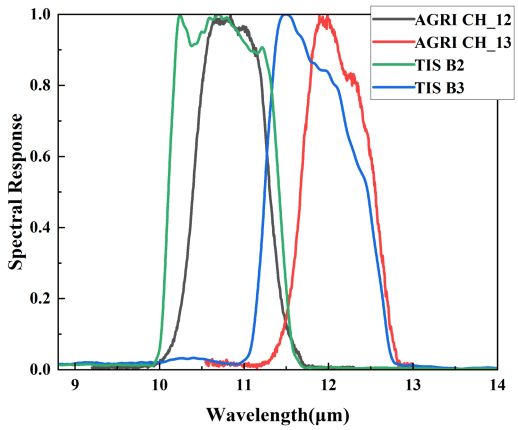

Fig. 1. Spectral response function of TIS and AGRI.

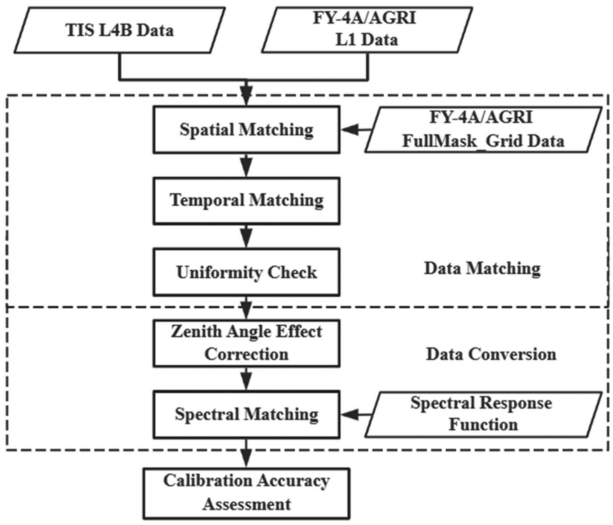

Fig. 2. Process of cross calibration.

infrared channels, completing a full-disk image within 30 min. AGRI provides full-disk scans within 15 min and rapid scans of China at 5-min intervals [4]. AGRI has stable performance, with the noise in the main infrared bands being better than 0.2 K when the target temperature is 300 K [5]. According to the results of daily and monthly cross calibration between AGRI and METOP C/infrared atmospheric sounding interferometer (IASI) by NSMC-GPRC (GSICS Processing and Research Center), the difference of BT between AGRIs CH_12 channel and IASI from 2022 to 2024 is less than 0.6 K, and the difference between CH_13 channel and IASI is less than 0.4 K. Given the spectral overlap between AGRI and TIS, as illustrated in Fig. 1, in this study, we use AGRI as the sensor for comparison with TIS.

II. DATA AND METHODS

The key factors influencing the accuracy of cross calibration include the consistency of spectral responses corresponding to each channel and the consistency of observational targets and geometric states [6]. The specific process of cross calibration is illustrated in Fig. 2, consisting primarily of three components: data matching, data conversion, and calibration accuracy assessment. The data used in the study are all from clear-sky conditions.

A. Data Matching

The data matching process involves aligning samples from cross-observed areas of two satellites and selecting suitable samples to ensure temporal, spatial, and geometric consistency as much as possible [7]. This is a critical step in the cross-calibration process, directly impacting the accuracy of cross calibration. We first resampled the TIS image, resulting in a spatial resolution of 4 km. By using the latitude and longitude information of the target image, projection calculations are performed to determine the row and column information of the target area. Therefore, when performing the spatial matching between TIS and AGRI, the minimum spatial area containing

the target TIS pixel can be determined based on the latitude and longitude information of the AGRI. Within this region, a point-by-point comparison is conducted to identify the most suitable AGRI pixel for matching. In addition, the uniformity of target features is another important factor influencing cross-calibration accuracy. As the FY-4A satellite is in a geostationary orbit (observing at 104.7°E subpoint) [8], clouds within the target area are constantly moving. To minimize uncertainties caused by spatial variations, only pixels from uniform scenes are chosen for cross calibration. The following formula is employed as a criterion to determine the uniformity of scenes:

$$\mathrm{RSTD}_{\mathrm{Target}} = \frac{\mathrm{STD}\,(\mathrm{Target})}{\mathrm{MEAN}\,(\mathrm{Target})} < \mathrm{max\_RSTD}_{\mathrm{Target}}. \quad (1)$$

In (1), Target represents the environmental region (5∗5 pixels), STD stands for standard deviation, MEAN denotes the mean value, $\mathrm{RSTD}_{\mathrm{Target}}$ indicates the relative standard deviation, and $\mathrm{max\_RSTD}_{\mathrm{Target}}$ serves as the threshold, with a selected value of $\mathrm{max\_RSTD}_{\mathrm{Target}} = 0.05$.

During cross calibration, the average radiance of AGRI within the region is compared with the average count value of TIS observations in DN. Using the environmental average helps mitigate the impact of positioning deviations. Following the data matching and uniformity checks, suitable matching samples for cross calibration of AGRI and TIS can be obtained.

B. FY-4A/AGRI Radiance Correction

Data conversion involves the correction of the radiance of FY-4A/AGRI and spectral matching operations.

Due to the sun-synchronous nature of TIS and its revisit cycle of 11 days, the quantity of simultaneously observed data samples under the FY-4A subpoint is limited. Therefore, considering the inclusion of large plateau lakes, such as Qinghai Lake, in the statistical data is essential to obtain absolute radiometric calibration accuracy results at observation points. In general, as the zenith angle increases, the path from the observation point to the satellite traverses a thicker atmospheric layer, leading to an increased atmospheric effect that affects the propagation and measurement of radiation [9]. To mitigate the influence of the atmosphere on radiation measurement results, we conducted simulations based on MODTRAN to obtain radiance under different observation zenith angle conditions. Using (2), the ratio of brightness temperature (BT) differences under different observation zenith angles is calculated

$$R_{\mathrm{VZA}\theta} = \frac{L_{\mathrm{VZA}\theta} - L_{\mathrm{VZA0}}}{L_{\mathrm{VZA0}}} \cdot 100\%. \quad (2)$$

In (2), $R_{\mathrm{VZA}\theta}$ represents the ratio of AGRI image radiance difference under satellite viewing zenith angle (VZA) θ, $L_{\mathrm{VZA}\theta}$ denotes the radiance value of AGRI image when the satellite observation zenith angle is θ, and L_{VZA0} represents the radiance value of the AGRI image at the satellite subpoint.

For the specific geometric differences introduced by the satellite observation zenith angle, this study conducts a quantitative analysis based on the trend of radiance differences with the change in zenith angle, as depicted in Fig. 3. By establishing a model for the satellite zenith angle–radiance difference ratio,

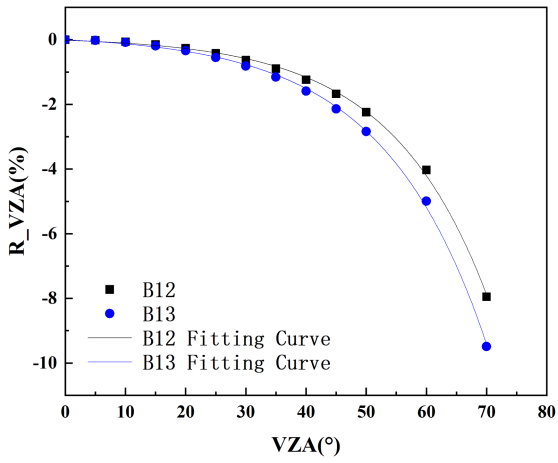

Fig. 3. Relationship between FY-4A/AGRI radiance difference ratio and VZA.

it is employed to analyze the impact of satellite zenith angle variations on radiance values, as expressed in (3). L_{correct} represents the radiance of FY-4A/AGRI corrected by the model

$$R_{\mathrm{VZA}}(\theta) = a + b \cdot e^{-\theta/c} \quad (3)$$

$$L_{\mathrm{correct}} = L \cdot (1 - R_{\mathrm{VZA}}(\theta)). \quad (4)$$

In (3), a, b, and c are the model coefficients, and their values are listed in Table II.

C. Calibration Accuracy Assessment

Spectral response matching is a crucial factor influencing the accuracy of cross calibration, as different spectral response functions can lead to varying response signals for the same input [10]. Using the MODTRAN atmospheric radiative transfer model, radiation spectral distributions under different atmospheric conditions are calculated to ensure that the selected samples cover a broad range of possible atmospheric scenarios. The simulated radiation spectral samples are convolved with the spectral response functions of TIS and AGRI, respectively, to obtain the corresponding radiance. The relationship between the radiance of AGRI and TIS radiance is established as follows:

$$L_{\mathrm{TIS}}^{B2} = A_1 \cdot L_{\mathrm{AGRI}}^{\mathrm{CH\_12}} + B_1 \quad (5)$$

$$L_{\mathrm{TIS}}^{B3} = A_2 \cdot L_{\mathrm{AGRI}}^{\mathrm{CH\_13}} + B_2 \quad (6)$$

where L_{AGRI} represents the radiance corrected by (4), and A and B denote the spectral matching factors obtained through the least squares method, which are listed in Table III.

The BT of TIS can be obtained through the inverse Planck function [11]

$$L_{\mathrm{TIS}} = k \cdot DN_{\mathrm{TIS}} + g \quad (7)$$

$$\mathrm{BT}_{\mathrm{TIS}} = \frac{K_2}{\ln\left(\frac{K_1}{L_{\mathrm{TIS}}} + 1\right)}. \quad (8)$$

TABLE II
COEFFICIENTS OF (3)

Atmosphere	Channel	a	b	c	R^2
Winter	12	0.08622	–0.10503	–16.16793	0.99902
	13	0.15910	–0.16232	–17.16599	0.99925
Summer	12	0.2301	–0.20772	–18.23054	0.99947
	13	0.36204	–0.3056	–19.83892	0.99966

TABLE III
VALUES OF THE SPECTRAL MATCHING FACTORS AND RADIOMETRIC CALIBRATION COEFFICIENTS OF TIS

Band of TIS	A	B	k	g	K_1/mW · cm^{-2} · sr^{-1} · μm^{-1}	K_2/K
B2	1.0202968	–0.1485301	0.003946	0.124622	838.7063	1342.7187
B3	1.1142946	–0.6917651	0.005329	0.222530	543.0580	1232.0214

TABLE IV
COMPARISON OF BT BIAS BEFORE AND AFTER CORRECTION

Observation Area	Qinghai Lake		Selincuo Lake		Namtso Lake	
Band	B2	B3	B2	B3	B2	B3
BT/K	288.55	288.00	281.84	281.04	284.71	284.73
BT bias before correction/K	–0.59	– 0.96	–1.03	–1.30	–1.19	–1.70
BT bias after correction/K	0.29	0.35	–0.31	–0.20	–0.53	–0.70

In (7), k and g represent the radiometric calibration coefficients of TIS, which are listed together with K_1 and K_1 in Table III.

The BT bias $\mathrm{BT}_{\mathrm{TIS-AGRI}}$ is obtained through (7)

$$\mathrm{BT}_{\mathrm{TIS-AGRI}} = \mathrm{BT}_{\mathrm{TIS}} - \mathrm{BT}_{\mathrm{AGRI}}. \tag{9}$$

III. RESULTS AND DISCUSSION

Based on the data and methods provided in Section II, we processed the TIR channel data from TIS and AGRI for the period from November 2021 to November 2023. Previous studies have already identified a correlation between BT bias and scene BT. Here, we utilize the local mean of statistical data to characterize the BT bias in the TIR channels of AGRI and TIS.

A. FY-4A/AGRI Radiance Correction Results

Equation (3) allows for the specific quantification of the channel BT error introduced by differences in satellite observation zenith angles. It is observed that when the observation zenith angle deviates by less than 15° from the nadir, the percentage difference in BT is approximately -0.05%, resulting in a channel BT error of about 0.15 K.

The satellite zenith angle–radiance correction model ensures that all other conditions remain constant except for the satellite observation zenith angle. At the Qinghai Lake observation point, the difference in satellite observation zenith angle is approximately 43°, at the Selincuo Lake, it is around 41°, and at Namtso Lake, it is approximately 39°. Selecting these locations with relatively similar zenith angle differences and minimal temporal differences for comparison before and after correction, it is observed that the BT differences are consistent after correction. The BT bias before and after correction is shown in Table IV, indicating that the BT differences after correction are significantly lower than those before correction.

B. TIS-AGRI BT Bias

Due to TIS being on a sun-synchronous satellite with an 11-day revisit cycle, the data sample size for observations under the FY-4A satellite is limited. In this study, while selecting data samples under the satellite subpoint (0°,104.7°E), as shown in Fig. 4, we utilized the radiance correction model described in (4) to correct non-sub-point data, thereby expanding the dataset. Non-sub-point data include observations from Qinghai Lake and Selincuo Lake. The reason for selecting data from these clear-sky, high-altitude lakes is to minimize the atmospheric impact on sensor radiance. The selected data are from January 2022 to February 2024, as shown in Figs. 5 and 6. Total 45 sets of TIS and AGRI data were used, with a total of 2250 samples.

Figs. 5 and 6 show the results of cross calibration of TIS using AGRI during daytime and nighttime, respectively. The BT bias for $B2$ and $B3$ is both within 1 K, with the standard deviation values of 0.22 K and 0.40 K in the daytime, and 0.31 K and 0.57 K at night.

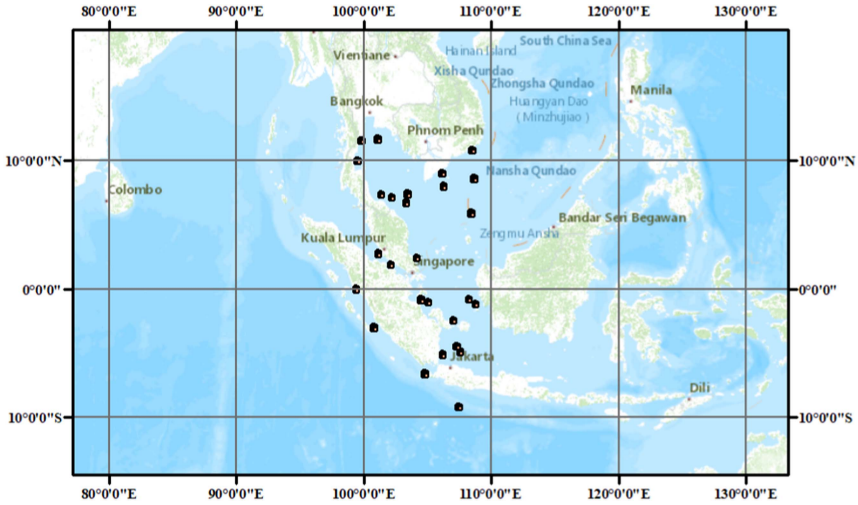

Fig. 4. Conceptual diagram of cross calibration between TIS and AGRI at subsatellite points.

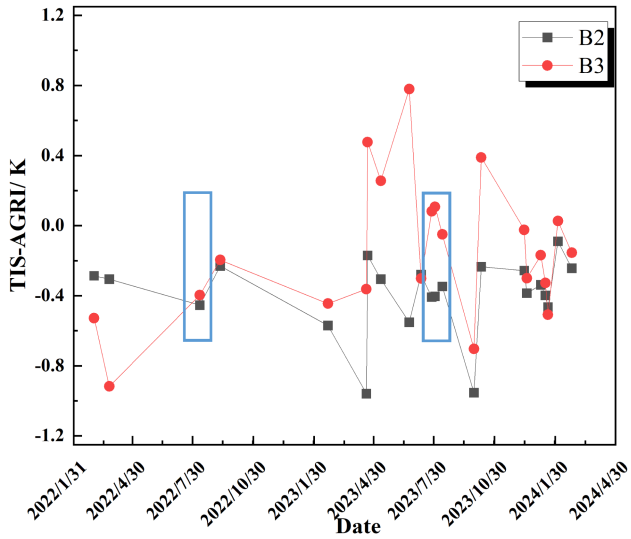

Fig. 5. Long-term periodic variation in BT bias of the *B*2 and *B*3 channels in the daytime.

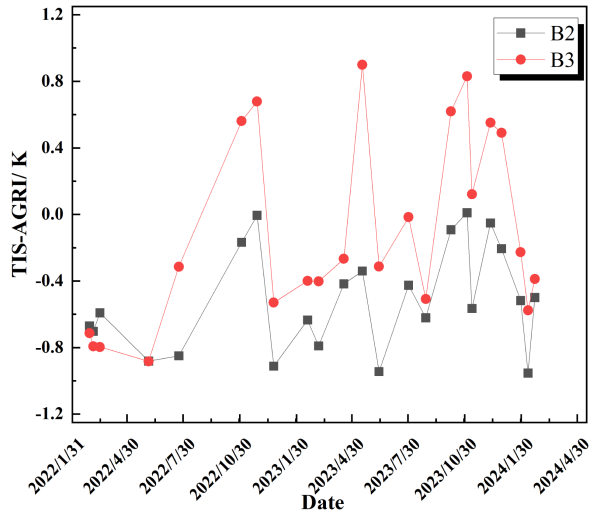

Fig. 6. Long-term periodic variation in BT bias of the *B*2 and *B*3 channels during the nighttime.

According to the results of cross calibration of FY-4A/AGRI with IASI, a well-calibrated hyperspectral radiometer, the BT bias between AGRI and IASI depends on the target temperature. For higher BTs, the bias is smaller and more stable, while it increases for lower BT values [8]. As depicted in Fig. 5, during summer, the differences in BTs between TIS bands *B*2 and *B*3 and those of FY-4A/AGRI remain within 0.5 K during the daytime, which is smaller than in other seasons. This is mainly because the target temperatures observed by the reference sensor FY-4A/AGRI are higher during summer daytime.

The nighttime BT bias for *B*2 and *B*3 channels is depicted in Fig. 6. The variation trend of BT bias between TIS and AGRI during the nighttime is consistent with the daytime trend.

The positive BT bias in the daytime of *B*3 is smaller than the BT bias at night. It was observed that the BT bias for band *B*2 exhibited negative differences during both daytime and nighttime, indicating that the BT of the TIS was lower than AGRI.

C. *Uncertainty Assessment*

The uncertainty of cross calibration is analyzed from the aspects of TIS instrument background response, MODTRAN simulation, TIS image resampling, and spectral response matching of TIS and AGRI.

For TIS radiometric calibration, since the first step in calculating incident radiance using the calibration equation is to remove the instrument's background response, the subsequent ability to apply high-precision radiance depends not only on the uncertainty of radiance calibration resulting from blackbody temperature calibration but also on the stability of the background response. By monitoring the response output of the blackbody temperature, the variation of the background response is observed, with stability higher than 0.1 K. According to the output from the 250 K blackbody, the uncertainty of the background response leads to a calibration accuracy of less than 0.2 K [12].

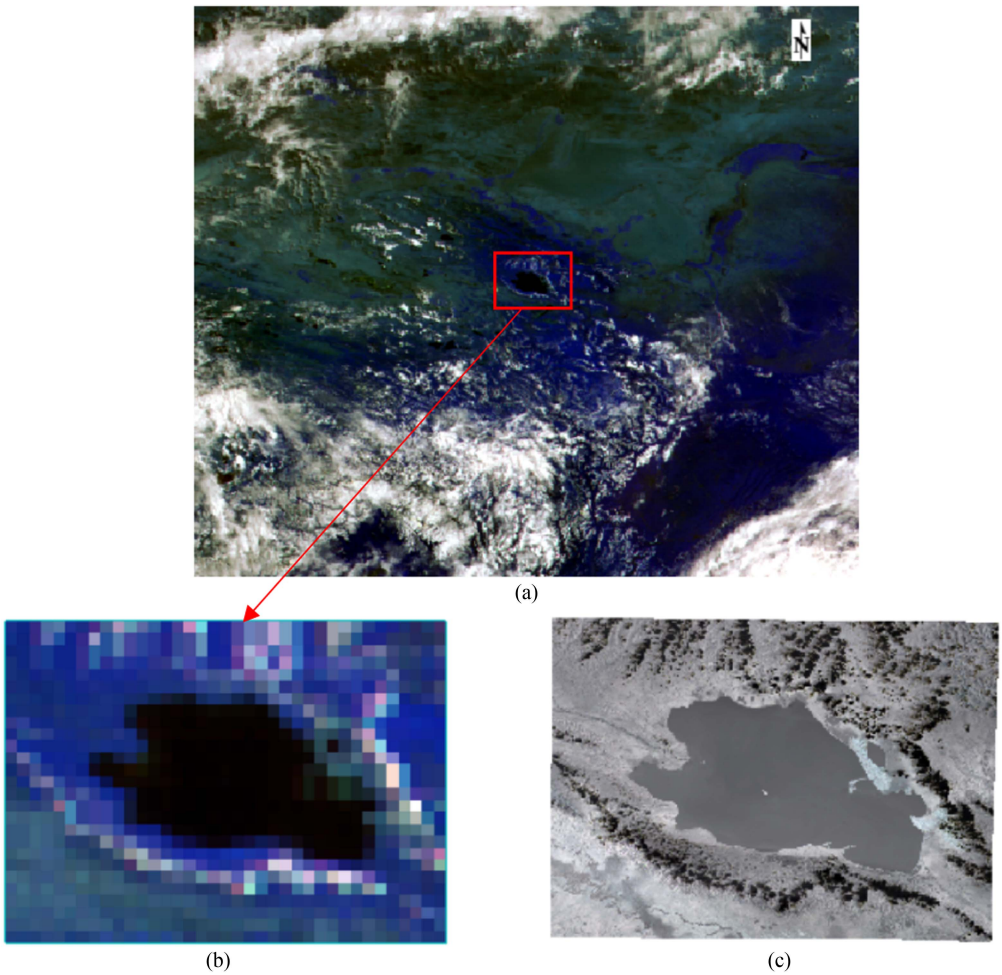

Fig. 7. Images (18 July 2023) captured by FY-4A and TIS in the Qinghai Lake region. (a) Image captured by FY-4A that includes the Qinghai Lake region. (b) FY-4A image in Qinghai Lake region. (c) TIS image in Qinghai Lake region.

TABLE V
RESULTS OF BT DEVIATION CALCULATIONS FOR THE QINGHAI LAKE REGION UNDER WINTER AND SUMMER ATMOSPHERIC CONDITIONS

Atmosphere	BT Bias of B2/K	BT Bias of B3/K
Midlatitude Winter	0.89	0.50
Midlatitude Summer	1.20	0.81
Difference	0.31	0.31

The satellite observation zenith angle radiance correction model is based on MODTRAN. Since it employs an atmospheric transmission model, this study provides a brief analysis of errors introduced by the atmosphere. The maximum error introduced by the atmosphere is calculated by considering the BT differences under two extreme conditions. Fig. 7 depicts the images of Qinghai Lake captured by FY-4A in the visible wavelength band and TIS. Table V presents the results of the BT bias calculations for the Qinghai Lake region (as shown in Fig. 7, captured by AGRI and TIS) under winter and summer atmospheric conditions, with the calculation coefficients, as listed in Table II.

The maximum BT uncertainty introduced by the atmospheric model is determined to be 0.31 K.

Due to the resampling of the TIS image, the spatial resolution of TIS has decreased to 4 km, which may introduce uncertainty in the calculation of BT bias for TIS-AGRI. In order to avoid the influence of satellite observation zenith angle on uncertainty estimation, we selected the TIS image near (0°,104.7° E) to evaluate the uncertainty. The selected sea surface data are relatively uniform. The uncertainty introduced by the resampling of $B2$ is 0.08 K, and the uncertainty of $B3$ is 0.09 K.

We analyzed the uncertainty of BT bias that may be introduced by spectral matching, as shown in Fig. 8. When analyzing the uncertainty introduced by spectral response matching, keeping the AGRI spectral response function unchanged, broadening and contracting the TIS spectral response function to change the spectral matching factor. The $B2$ band is less affected by spectral

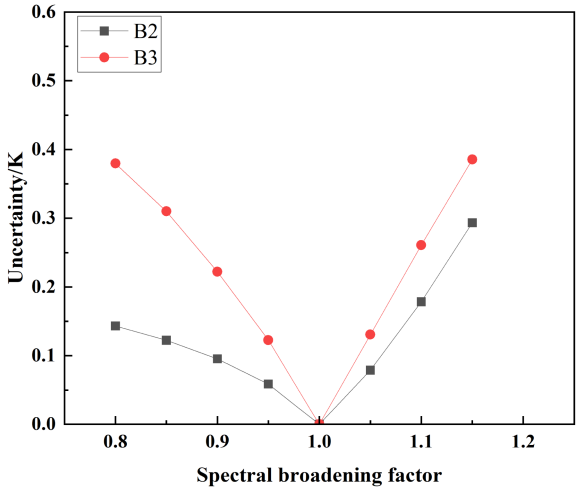

Fig. 8. Uncertainty of BT bias introduced by spectral matching of TIS and AGRI.

response matching than *B*3. When the spectral broadening is 1.15 times the wavelength interval, the uncertainty of *B*2 is less than 0.29 K and *B*3 is less than 0.38 K.

IV. Conclusion

The article discusses the long-term on-orbit radiometric calibration accuracy comparison between FY-4A/AGRI and SDGSAT-1/TIS. Due to AGRIs' observations at the nadir point under the E104.7° longitude satellite, and SDGSAT being a sun-synchronous orbit satellite with limited data at the nadir point, a radiance correction model for FY-4A/AGRI is proposed in this study. This model can to some extent mitigate the impact of geometric inconsistencies between AGRI and TIS observations, enabling the utilization of data from uniform regions, such as Qinghai Lake, Selincuo Lake, and Namtso Lake.

Through long-term observations, it was found that the BT bias for *B*2 and *B*3 remained within 1 K. Overall, the on-orbit calibration accuracy of TIS using AGRI for monitoring is satisfactory. During the daytime in summer, when target temperatures are higher, the BT bias is within 0.5 K, which may be due to the higher precision of FY-4A/AGRI observations when targeting higher temperatures. Error calculations for Qinghai Lake data introduced into the model are performed under summer and winter atmospheric conditions. The calculated model-induced uncertainty is found to be less than 0.31 K and the uncertainty introduced by spectral matching is less than 0.4 K.

Acknowledgment

The authors would like to thank the International Research Center of Big Data for Sustainable Development Goals (CBAS) and National Space Science Center, the Chinese Academy of Sciences for sharing the TIS data, and also Fengyun Satellite Remote Sensing Data Service Network for providing the FY-4A/AGRI data. The opinions in this article are entirely the authors' own.

References

[1] Z. Hu, M. Zhu, Q. Wang, X. Su, and F. Chen, "SDGSAT-1 TIS prelaunch radiometric calibration and performance," *Remote Sens.*, vol. 14, no. 18, Sep. 2022, Art. no. 4543.

[2] C. Gao et al., "Radiometric cross-calibration of GF-4/VNIR sensor with Landsat8/OLI, Sentinel-2/MSI, and Terra/MODIS for monitoring its degradation," *IEEE J. Sel. Topics Appl. Earth Observ. Remote Sens.*, vol. 13, pp. 2337–2350, May 2020.

[3] B. Zhong, Y. Ma, A. Yang, and J. Wu, "Radiometric performance evaluation of FY-4A/AGRI based on aqua/MODIS," *Sensors*, vol. 21, no. 5, Mar. 2021, Art. no. 1859.

[4] L. Sun et al., "On-orbit calibration analysis of FY-4A AGRI solar bands," *Proc. SPIE*, vol. 10781, Oct. 2018, Art. no. 1078110.

[5] B.-Y. Chen, Q. Wu, X. Feng, Q. Guo, and C.-Y. Wei, "On-orbit test to FY-4A AGRI and generating RBG image," *J. Infrared Millimeter Waves*, vol. 37, no. 4, pp. 411–415, Aug. 2018.

[6] J. Han, Z. Tao, Y. Xie, H. Li, Q. Liu, and X. Guan, "A novel radiometric cross-calibration of GF-6/WFV with MODIS at the Dunhuang Radiometric calibration site," *IEEE J. Sel. Topics Appl. Earth Observ. Remote Sens.*, vol. 14, pp. 1645–1653, 2021.

[7] W. Liu, J. Li, Q. Han, L. Zhu, H. Yang, and Q. Cheng, "Orbital lifetime (2008–2017) radiometric calibration and evaluation of the HJ-1B IRS thermal infrared band," *Remote Sens.*, vol. 12, no. 15, Aug. 2020, Art. no. 2362.

[8] X. He, N. Xu, X. Feng, X. Hu, H. Xu, and Y. Peng, "Assessing radiometric calibration of FY-4A/AGRI Thermal infrared channels using CrIS and IASI," *IEEE Trans. Geosci. Remote Sens.*, vol. 60, 2022, Art. no. 5514512.

[9] H. Gao, X. Gu, T. Yu, Y. Sun, and Q. Liu, "Cross-calibration of GF-1 PMS sensor with Landsat 8 OLI and Terra MODIS," *IEEE Trans. Geosci. Remote Sens.*, vol. 54, no. 8, pp. 4847–4854, Aug. 2016.

[10] Y. Li, X. Xiong, J. McIntire, and A. Wu, "Comparison of the MODIS and VIIRS thermal emissive band radiometric calibration," *IEEE Trans. Geosci. Remote Sens.*, vol. 58, no. 7, pp. 4852–4859, Jul. 2020.

[11] M. Liu, L. Guan, J. Liu, Q. Song, C. Ma, and N. Li, "First assessment of HY-1C COCTS thermal infrared calibration using MetOp-B IASI," *Remote Sens.*, vol. 13, no. 4, Feb. 2021, Art. no. 635.

[12] Z. Hu et al., "Wide-swath and high-resolution whisk-broom imaging and on-orbit performance of SDGSAT-1 thermal infrared spectrometer," *Remote Sens. Environ.*, vol. 300, Jan. 2024, Art. no. 113887.

Min Zhu received the B.S. degree in communication engineering from the Ocean University of China, Qingdao, China, in 2019. She is currently working toward the Ph.D. degree in electronic circuits and systems with the Shanghai Institute of Technical Physics, Chinese Academy of Sciences, Shanghai, China, and the University of Chinese Academy of Sciences, Beijing, China.

Her current research interests include the radiometric calibration method of multidimensional photoelectric system and cross calibration.

Xue Zhao received the B.S. degree in mechanical engineering from Hangzhou Dianzi University, Hangzhou, China, in 2022. He is currently pursuing the Ph.D. degree in physical electronics at Shanghai Institute of Technical Physics of Chinese Academy of Sciences, University of Chinese Academy of Sciences, Beijing, China.

His current research interests include high-precision radiation calibration of infrared instruments in orbit combined with artificial intelligence.

Lu Zou received the B.S. degree in physics electronics from the Beijing Institute of Technology, Beijing, China, in 2010.

His research interests include infrared target detection and target recognition.

Fansheng Chen received the B.S. degree in optoelectronic information engineering from Shandong University, Jinan, China, in 2002, and the Ph.D. degree in physical electronics from the Shanghai Institute of Technical Physics, Chinese Academy of Sciences, Shanghai, China, in 2007.

Since 2013, he has been a Professor with the Shanghai Institute of Technical Physics, Chinese Academy of Sciences. His research interests include the design of spatial high-resolution remote sensing and detection payloads, high-speed and low-noise information acquisition technology, and infrared dim small target detection technology. Meanwhile, he has been committed to the research and development of the space infrared staring detection instruments, the high spatial and temporal resolution photoelectric payloads, and the application of infrared multispectral information acquisition technology in artificial intelligence, target recognition, and other relative aspects.

Zhuoyue Hu received the B.S. degree in information display and optoelectronic technology from the University of Electronic Science and Technology of China, Chengdu, China, in 2016, and the Ph.D. degree in physical electronics from the Shanghai Institute of Technical Physics, Chinese Academy of Sciences, Shanghai, China, in 2021.

Her research interests include the radiometric calibration of remote sensing satellites.